

# Energy dissipation characteristics of sandstone cutting under mechanical impact load

Wang Shuren<sup>1\*</sup>, Su Junqing<sup>1</sup>, Hagan Paul<sup>2</sup>

<sup>1</sup>School of Civil Engineering and Mechanics, Yanshan University, Qinhuangdao, 066004, China

<sup>2</sup>School of Mining Engineering, University of New South Wales, Sydney, 2052, Australia

Received 28 march 2014, www.tsi.lv

---

## Abstract

Based on the sandstone experiment by using the linear rock cutting machine at the school of mining engineering, University of New South Wales (UNSW), the computational model was built by using particle flow code (PFC), and the energy dissipation characteristics was studied considering these parameters such as cutting speed, cutting depth, rock strength, rock temperature and rock confining pressure. The results showed that the specific energy and acoustic emission of sandstone were proportional to the cutting speed and rock strength, there was an optimal depth of rock cutting with the cutting depth increasing under the confining pressure condition, and the specific energy and acoustic emission of sandstone changed obviously due to the influence of the rock temperature and rock confining pressure.

*Keywords:* Rock Cutting, Energy Dissipation, Specific Energy, Acoustic Emission, Particle Flow Code

---

## 1 Introduction

Rock-cutting usually caused the process of initiation crack, development, expansion, aggregation and transfixion of micro fissures in the rock under dynamic loading [1]. For the difficulty degree and energy dissipation of rock-cutting, they are not only the important indicators to evaluate the drilling, blasting, mining, beneficiation process, but also the key parameters to optimize the rock fragment and improve the production capacity.

At present, many domestic scholars have done lots of work in evaluating the difficulty of rock -cutting and energy dissipation, and achieved fruitful research results [2-3]. For example, X.B. Li et al. had conducted the impact crushing tests on four kinds of typical rocks under different loading waveforms, and found that the amount of energy absorbed by the rock was the most under the bell-wave loading [4]. M.Q. You et al. conducted the conventional triaxial loading test, and proved that the amount of energy absorbed by the broken rock was increased in a linear manner with increasing confining pressure [5]. C.J. Xia et al. had carried out the impact experiments of man-made rock with different porosities with Split Hopkinson Pressure Bar (SHPB), the characteristic of energy dissipation and the influence of rock porosity on energy dissipation were investigated during the impact process, and the relationship between the energy dissipation of critical failure and rock porosity was also analysed [6]. Q. Su et al. researched the mechanism of sand energy dissipation under the cyclic loading using particle flow code (PFC), and proved that

the smaller the sand porosity, the more system energy dissipation, and the energy dissipation improved with the confined pressure increasing [7]. For the research of specific energy of rock breaking, the main representative theories were put forward by foreign scholars such as the new-surface theory (P.R. Rittingerde), the similarity theory (G. Kick) and the crack theory (F.C. Bond) [8]. R.M. Goktan et al. researched the relationship between the rock brittleness index and rock-cutting efficiency, and found that the rock-cutting efficiency improved with the rock brittleness increasing under other conditions remained unchanging [9]. H. Copur et al. developed a set of new empirical indices and a new interpretation method of macro-scale indentation tests, which were useful for predicting the cutting efficiency and mechanical properties of rocks [10]. B. Adebayo made an assessment of the cuttability of granite and limestone, and found that the cutting rate increased in a linear manner with the growth of rebound hardness value, uniaxial compressive strength and silica content [11]. K. Dey et al. had proposed a new index, which could reasonably predict the production efficiency of the surface coal mining [12]. D. Tumac et al. tried to evaluate the cuttability of rocks by using the rock hardness and the uniaxial compressive strength index [13], and the related studies [14-15], etc.

In summary, though many research achievements have been obtained for evaluating the difficulty of rock breaking and energy dissipation, there is still a lot of work to be researched in depth due to the non-uniformity of rock material, the difference of geological conditions and the complexity of engineering conditions. Therefore, the numerical calculation model of rock-cutting was built

---

\* Corresponding author e-mail: w\_sr88@163.com

based on the test by using the linear rock-cutting equipment at the University of New South Wales (UNSW) in Australia. The numerical simulation of rock-cutting energy dissipation was conducted under different conditions, which was of important theoretical significance and practical value in guiding the similar engineering to reduce the cost of drilling and blasting and improve the production efficiency.

## 2 Rock-cutting experiment under the impact load

### 2.1 TESTING EQUIPMENT AND SAMPLES

The cutting test was conducted by using the linear rock cutting machine in the laboratory of School of Mining Engineering (UNSW). As shown in Fig. 1, the dimensions of the cutting machine were 1829 mm long, 1118 mm wide and 1321 mm high, respectively.

All the sandstone samples were obtained from the field adjacent to hynds seam in Hunter Valley, New South Wales. For each cutting test, the dynamic monitor fixed on the cutter monitored the voltage change data along the horizontal cutting direction and vertical cutting direction (Fig. 1), the mechanical impact curves of cutting force and normal force could be shown on the computer screen in real time through the conversion software program. For each sandstone sample, the cutting test should be operated for four times orderly, as showed in Fig. 1(c).

### 2.2 TEST METHODS AND PROCEDURES

The process of the test was as follows:

Step 1: Each cylindrical core sample with diameter  $\varnothing 76$  mm should be fixed in the planer with flat clamp horizontally.

Step 2: Installing the new standard cutting tool, which was 12.5 mm wide chisel with front rake angle  $0^\circ$ , back clearance angle  $5^\circ$ , and cemented tungsten carbide.

Step 3: Adjusting the cutter depth of 5 mm through raising or lowering the lathe height. A flat tray was prepared for collecting cutting debris, and the testing machine must be covered with transparent plastic sheeting to prevent debris scattered everywhere.

Step 4: Starting the testing machine to cut the sandstone sample at a constant speed of 150 mm/s. During the test, the sandstone sample should be rotated counter clockwise by  $180^\circ$  after the first cutting being finished, then the second cutting can be operated along the same direction as the first cutting. After the second

cutting it should be rotated counter clockwise by  $90^\circ$  according to the position of the first cutting and the third cutting should be conducted. Finally, the sandstone sample should be rotated counter clockwise by  $180^\circ$  according to the third cutting and the forth cutting should be completed [16].

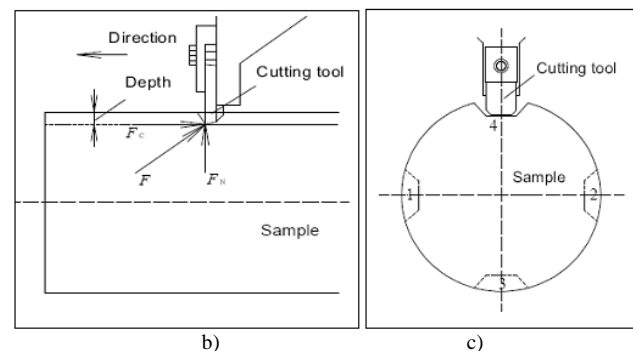


FIGURE 1 Linear rock-cutting machine and cutting sequence diagram: a) Testing machine and test system, b) Side view of sample, c) Front view of sample.

### 2.3 EXPERIMENT RESULTS AND ANALYSIS

#### 2.3.1 Fragment characteristics of cutting debris

Fig. 2 showed the four sandstone samples and the collected rock-cutting debris, respectively. For each rock sample and for each cutting, the cutting debris must be collected, bagged, numbered and weighted. From the test results we found that samples No. 377542 and No. 377590 were short, their recovery ratios were low, their cleavage and cranny were developed, so the integrity was poor. On the contrary, samples No. 377554 and No. 370526 were long, their recovery ratios were high, their cleavage and cranny were not developed, and the integrity was good.



FIGURE 2 Sandstone samples and rock-cutting debris: a) No. 377542, b) No. 377554, c) No. 370526, d) No. 377590

2.3.2 Specific energy analysis of cutting debris

In the experiment, the specific energy (*SE*) is the energy or work required to cut unit volume of the rock, then *SE* is calculated as follows:

$$SE = \frac{F_c}{V} \tag{1}$$

Where  $F_c$  is the mean cutting force (kN), and  $V$  is the volume of excavated material per unit length of cutting ( $m^3/km$ ). The unit of *SE* is usually  $MJ/m^3$ .

$$V = LS \tag{2}$$

Where  $L$  is the distance the pick travels (m), and  $S$  is the unit cross-sectional area along the pick travels ( $m^2$ ).

In a given rock the specific energy is used as a measure of the efficiency of a cutting system with lower values indicating higher efficiency, and what's more, in the context of cuttability assessment, it can be used to both compare the cuttability of different rocks and indicate approximately the potential excavation rate for a particular machine type in a given rock [17]. Table 1 showed the mean cutting force, the mean normal force and the specific energy of rock-cutting on the basis of the experimental data statistics by using the linear rock-cutting equipment.

As seen from Figs. 3 and 4, with the curves of the mean values changed from high to low, it indicated that the strength of the four types of sandstones changed from high to low. That is, the specific energy of rock-cutting increased with the growth of rock strength, and vice versa.

TABLE 1 Parameter statistics of the rock-cutting experiment

Sample	Cutting sequence	Cutting force (kN)	Normal force (kN)	Distance (mm)	Specific quantity ( $m^3/km$ )	Specific energy ( $MJ/m^3$ )
a) 377542	RTC14	1.56	1.62	180	0.0534	29.28
	RTC15	1.56	1.54	326	0.0738	21.17
	RTC16	1.78	1.87	486	0.0793	22.47
	RTC17	2.51	2.68	611	0.0615	40.78
	<b>Mean</b>	<b>1.85</b>	<b>1.93</b>	<b>401</b>	<b>0.067</b>	<b>28.43</b>
b) 377554	RTC30	1.77	1.62	180	0.0711	24.96
	RTC31	1.82	1.63	198	0.0666	27.29
	RTC32	1.80	1.63	208	0.0671	26.79
	RTC33	1.28	1.25	190	0.0665	26.79
	<b>Mean</b>	<b>1.67</b>	<b>1.53</b>	<b>194</b>	<b>0.068</b>	<b>26.46</b>
c) 370526	RTC34	1.31	1.09	218	0.0640	20.47
	RTC35	1.21	1.01	437	0.0566	21.32
	RTC36	1.37	1.06	647	0.0720	19.00
	RTC37	1.35	1.01	863	0.0682	19.77
	<b>Mean</b>	<b>1.31</b>	<b>1.04</b>	<b>541</b>	<b>0.065</b>	<b>20.14</b>
d) 377590	RTC53	0.75	0.58	162	0.0940	7.95
	RTC54	1.15	0.78	322	0.1489	7.75
	RTC55	0.79	0.62	458	0.0517	15.32
	RTC56	0.81	0.63	593	0.0897	8.98
	<b>Mean</b>	<b>0.88</b>	<b>0.65</b>	<b>384</b>	<b>0.096</b>	<b>10.00</b>

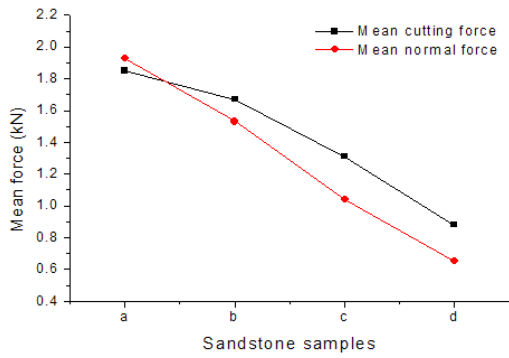


FIGURE 3 Curves of mean force changing

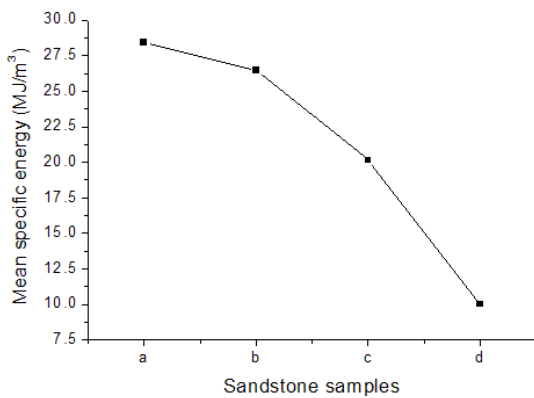


FIGURE 4 Curves of mean specific energy changing

### 3 Rock-cutting numerical test under the impact load

#### 3.1 BUILDING COMPUTATIONAL MODEL

As shown in Figs. 5 and 6, the numerical calculation model was built by using PFC according to the engineering mechanical model. The horizontal velocity of the calculation model was zero, the top surface was free or the confining pressure boundary. The cutter simulated by using two mutually perpendicular wall sections was moved to the right at a certain velocity, the back-rake angle and the cutting depth to simulate the cutting process.

The specific process of modelling was as follows:

Step 1: The specimen was rectangular (width × height = 100 mm × 50 mm) and confined by three frictionless walls on the bottom, the left and the right sides, which was generated by the radius expansion method.

Step 2: The radii of all particles were changed uniformly to achieve a specified isotropic stress so as to reduce the magnitude of locked-in stresses that would develop after the subsequent bond-installation. In this paper the isotropic stress was set to 0.1 MPa.

Step 3: The floating particles that have less than three contacts were eliminated. Then the parallel bonds were installed throughout the assembly among all particles. The cutter was represented by two wall segments (both of length  $l = 80$  mm) that were mutually perpendicular with

a back-rake angle of  $20^\circ$ . The cutter was moved horizontally across the rock at a velocity of 0.5 m/s and at a cutting depth of 5 mm.

Step 4: In order to simulate the compressive stress on the rock surface, a pressure-application algorithm is developed for PFC by continually identifying a connected chain of particles on the rock surface, and applying the pressure to those particles as the cutting process proceeds.

Step 5: In the process of rock-cutting simulation, the calculation model could trace energy data through the built-in energy function in PFC, and record the crack data through the built-in crack function so as to monitor the variation of rock temperature, specific energy and acoustic emission.

Step 6: The variation law of specific energy and acoustic emission would be analysed statistically with the change of the cutting speed, the cutting depth, the rock temperature and the confined pressure.

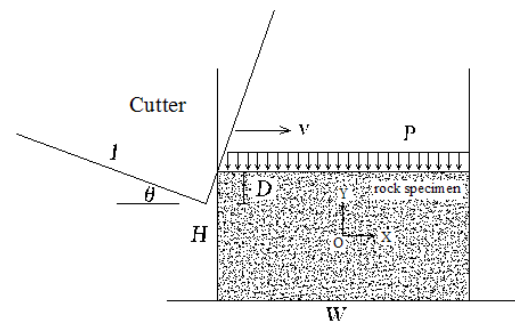


FIGURE 5 Engineering mechanic model of rock-cutting

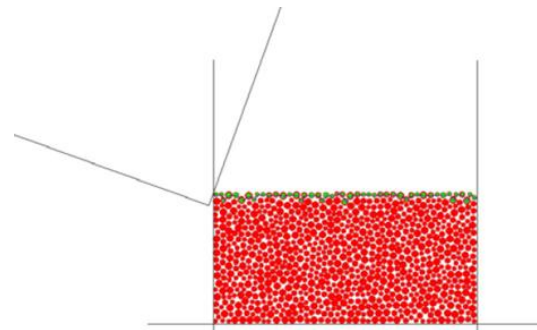


FIGURE 6 Computational model of rock-cutting

#### 3.2 PARAMETERS CALIBRATION OF THE ROCK SPECIMEN

The rock specimen was treated as the porous material that consisted of particles and the cemented bodies. Before the numerical test, the micro mechanical parameters should be adjusted repeatedly until these parameters were consistent with the physical experiment results.

The micro mechanical required to be adjusted are as follows:  $\rho_{bulk}$  is bulk density,  $R_{max}/R_{min}$  is ball size ratio,  $R\_ratio$  is ball size ratio,  $\mu$  is ball friction coefficient,  $\bar{\lambda}$  is parallel-bond radius multiplier,  $E_c$  is ball-ball contact modulus,  $\bar{E}_c$  is parallel-bond modulus,  $k_n/k_s$  is

ball stiffness ratio,  $\bar{k}_n/\bar{k}_s$  is parallel-bond stiffness ratio,  $\bar{\sigma}_c$  is parallel-bond normal strength,  $\bar{\tau}_c$  is parallel-bond

shear strength. The micro-parameters of the model were listed in the Table 2.

TABLE 2 Micro mechanical parameters of the model in PFC

$\rho_{bulk}$ (kg/m <sup>3</sup> )	$R_{max}/R_{min}$	$R\_ratio$	$\mu$	$\bar{\lambda}$	$E_c$ (Pa)	$\bar{E}_c$ (Pa)	$k_n/k_s$	$\bar{k}_n/\bar{k}_s$	$\bar{\sigma}_c$ (Pa)	$\bar{\tau}_c$ (Pa)
2620	1.66	1.66	0.5	1.0	83e9	83e9	3.8	3.8	91e6	91e6

3.3 ROCK-CUTTING ENERGY CHARACTERISTICS

3.3.1 Specific energy variation with the cutting velocity

As shown in Fig. 7, the specific energy of rock-cutting was proportional to the cutting velocity. The specific energy under the confined pressure was greater than that without the confined pressure at the same cutting velocity. What was more, as a result of the effect of the confined pressure, the curve slope was greater, that is, the specific energy of rock-cutting increased faster with the cutting velocity increasing under the confined pressure condition.

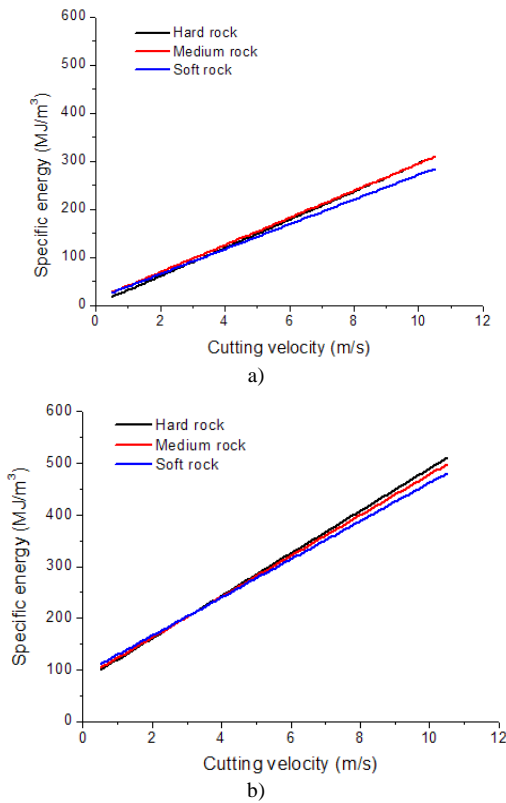


FIGURE 7 Specific energy-cutting velocity variation curves: a) without the confined pressure, b) with the confined pressure P = 10 MPa

Fig. 7(a) showed that the specific energy of the hard rock increased the fastest, followed by the medium hard rock, the last was the soft rock with the cutting velocity increasing without the confined pressure. Fig. 7(b) showed that the slope of curve, the value of specific energy and the amount of energy consumption increased obviously under the confined pressure being set to 10 MPa.

3.3.2 Specific energy variation with the cutting depth

As shown in Fig. 8(a), with the cutting depth increasing, the specific energy curves of three kinds of sandstones presented the slow-growth trend without the confined pressure, while the medium hard rock began to decline when the cutting depth was at 20 mm. As shown in Fig. 8(b), under the confined pressure, with the cutting depth increasing, the specific energy curves decreased at first and then increased. There was a minimum value of specific energy, which was called the optimal rock-cutting depth. The optimal rock-cutting depth of hard rock was about 18 mm, that of the medium hard rock was about 24 mm, and that of the soft rock was about 21 mm.

Compared Fig. 8(a) and Fig. 8(b), we could find that the cutting depth should not be too deep for hard rock and soft rock, while the cutting depth of the medium hard rock could increase appropriately.

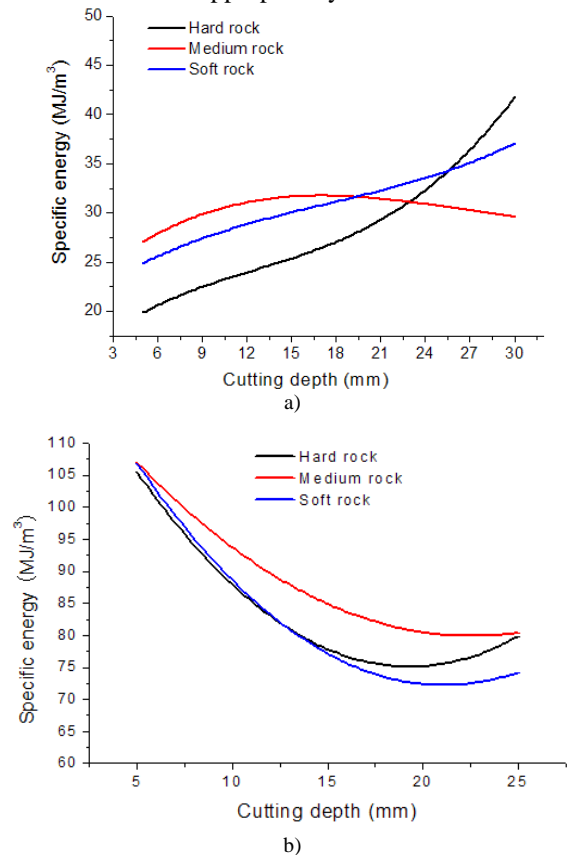


FIGURE 8 Specific energy-cutting depth variation curves: a) without the confined pressure, b) with the confined pressure P = 10 MPa

3.3.3 Specific energy variation with the rock temperature

As shown in Fig. 9, with the rock temperature increasing, the specific energy curves of three kinds of sandstones demonstrated S-shaped nonlinear change at the low value without the confined pressure, and the soft rock changed obviously than the others. After applying the confined pressure, the specific energy curves of hard rock and soft rock demonstrated S-shaped nonlinear change at the high value, while the medium hard rock changed greatly than the others.

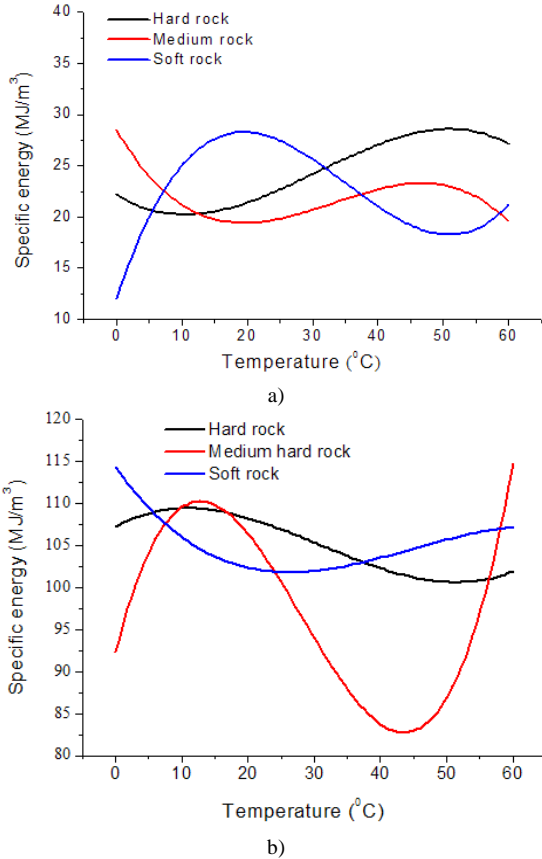


FIGURE 9 Specific energy-temperature variation curves: a) without the confined pressure, b) with the confined pressure P = 10 MPa

Compared Fig. 9(a) and Fig. 9(b), we find that the specific energy under the confined pressure at 10 MPa was about five times larger than that without the confined pressure.

3.4 ROCK-CUTTING AE CHARACTERISTICS

3.4.1 Acoustic emission variation with cutting velocity

The acoustic emission (AE) is commonly defined as transient elastic waves within a material caused by the release of localized stress energy. The rock AE is directly related to the generation of internal micro cracks (damage). A micro crack occurs along with a release of strain energy, that is, there is an AE. Therefore, the rock AE can be simulated by recording number of micro cracks. So the crack function defines a link damage

between particles as a crack generation in PFC. As a result, the rock AE can be simulated by the crack function in PFC.

As shown in Fig. 10, the AE was directly proportional to the cutting velocity. Without the confined pressure, there was an obvious difference among the growth rate of the AE three kinds of sandstones, while under the confined pressure, the growth rate of the AE were almost the same.

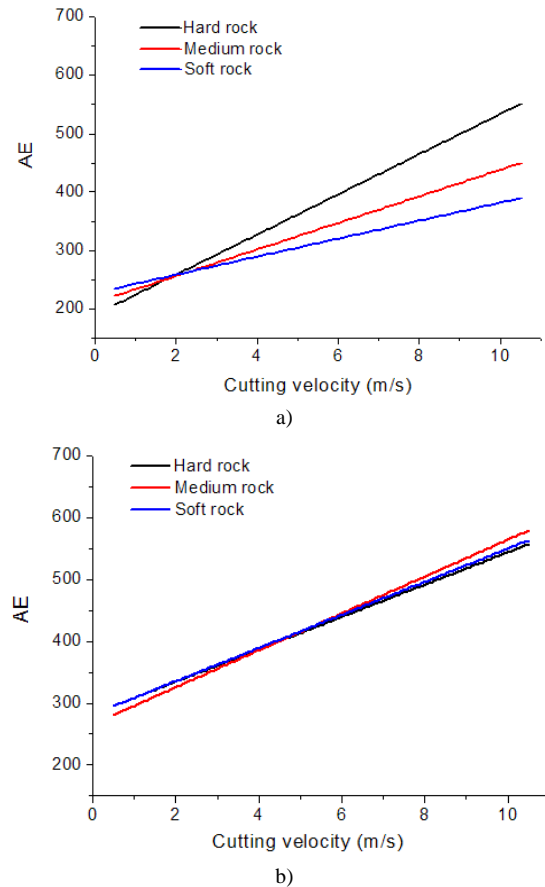


FIGURE 10 Specific energy-AE variation curves: a) without the confined pressure, b) with the confined pressure P = 10 MPa.

As shown in Fig. 10(a), with the cutting velocity increasing, the AE growth rate of the hard rock increased the fastest, followed by the medium hard rock and the last was the soft rock. When the cutting velocity was less than 2.0 m/s, the growth rate of AE was soft rock>medium hard rock>hard rock; When the cutting velocity was more than 2.0 m/s, the growth rate of AE was hard rock>medium hard rock>soft rock. As shown in Fig. 11(b), after being set the confined pressure at 10 MPa, the growth rate of AE of three kinds of sandstones were almost the same.

3.4.2 Acoustic emission variation with the cutting depth

As shown in Fig. 11, with the cutting depth increasing, the confined pressure only had a slight influence on the AE growth rate of the medium hard rock, and it had no effect on that of the hard rock and the soft rock. In a

word, no matter whether the confined pressure existed or not, the hard rock had the same AE growth rate as that of the soft rock.

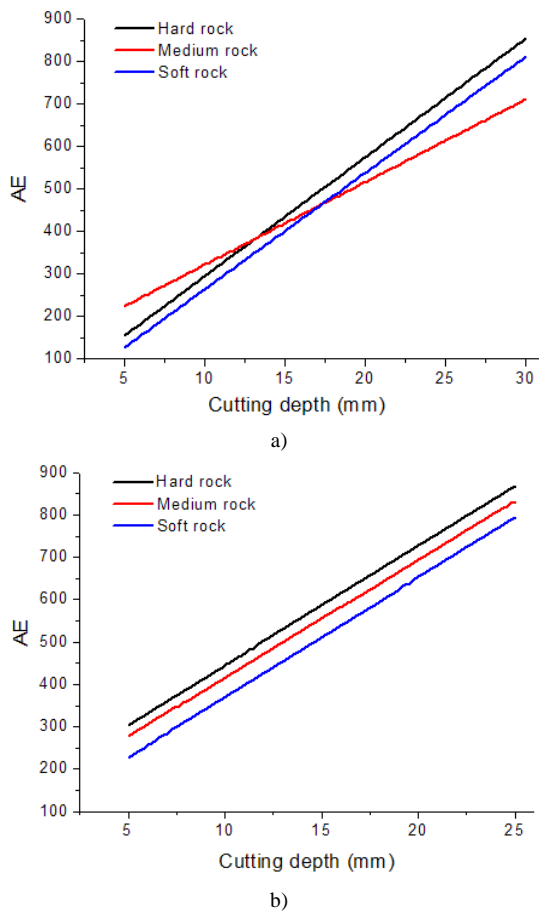


FIGURE 11 Cutting depth-AE variation curves: a) without the confined pressure, b) with the confined pressure P = 10 MPa

As shown in Fig. 11(a), without the confined pressure, the number of AE was proportional to the cutting depth. The AE growth rate of the hard rock was equal to the soft rock and greater than the medium hard rock. The curves in Fig. 11(b) showed that three kinds of sandstones AE were proportional to the cutting depth, and had the same slope, namely the growth rates were equal under the confined pressure. The AE of three kinds of sandstones had the following relationship: the hard rock was the greatest, followed by the medium hard rock and the last was the soft rock.

### 3.4.3 Acoustic emission variation with the rock temperature

As shown in Fig. 12(a), with the rock temperature increasing, the AE of the hard rock and the medium hard rock had little changes, while the soft rock increased at first and then decreased without the confined pressure within the temperature range of 0 °C to 60 °C, and reached the maximum value at 30 °C.

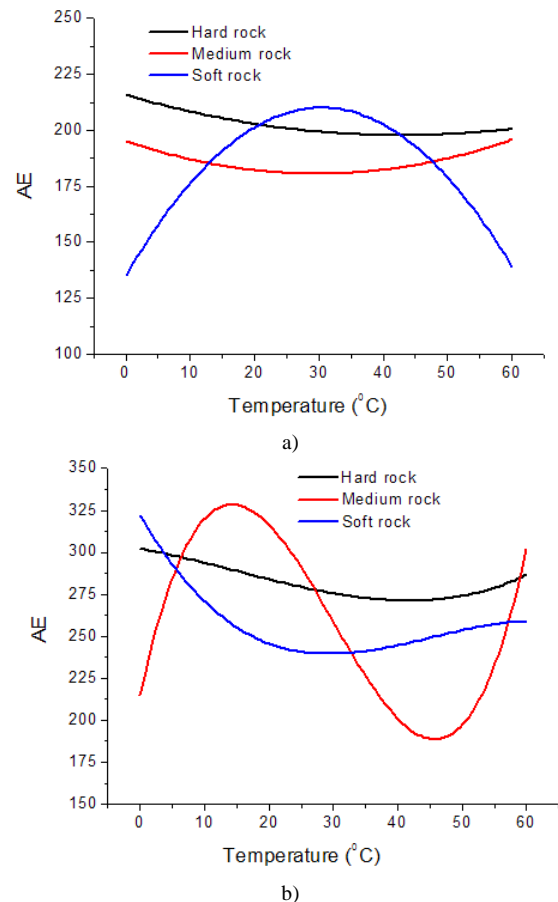


FIGURE 12 Rock temperature-AE variation curves: a) without the confined pressure, b) with the confined pressure P = 10 MPa

The curves in Fig. 12(b) showed that the AE of the hard rock and the soft rock presented a slowly downward trend and remained the same above 30 °C. And the medium hard rock was greatly influenced by the temperature factors, of which the curve presented an inverted S-shaped and obtained the maximum value at about 15 °C and reached the minimum value at about 45 °C.

## 4 Conclusion

The specific energy of rock-cutting was proportional to the cutting velocity. With the cutting depth increasing, the specific energy curves of three kinds of sandstones presented the slow-growth trend without the confined pressure, while the medium hard rock began to decline when the cutting depth at a certain value. Under the confined pressure, with the cutting depth increasing, the specific energy curves decreased at first and then increased and there was an optimal depth of rock cutting.

With the rock temperature increasing, the specific energy curves of three kinds of sandstones demonstrated S-shaped nonlinear change at the low value without the confined pressure, and the soft rock changed obviously than the others. After applying the confined pressure, the specific energy curves of hard rock and soft rock demonstrated S-shaped nonlinear change at the high

value, while the medium hard rock changed greatly than the others.

AE was directly proportional to the cutting velocity and the cutting depth. With the rock temperature increasing, the AE curves of three kinds of sandstones demonstrated nonlinear change.

## References

- [1] Lin D N, Chen S R 2005 Experimental study on damage evolution law of rock under cyclical impact loadings *Chinese Journal of Rock Mechanics and Engineering* **24**(22) 4094-4098 (in Chinese)
- [2] Hu L Q, Li X B, Zhao F J 2002 Study on energy consumption in fracture and damage of rock induced by impact loadings *Chinese Journal of Rock Mechanics and Engineering* **S2** 2304-2308 (in Chinese)
- [3] Guo L J, Yang Y H, Hua Y H 2013 Test and analysis on distortion and damage of rock under impact loading *Journal of Water Resources and Architectural Engineering* **11**(6) 31-34 (in Chinese)
- [4] Li X B, Lai H H, Gu D S 1992 Energy consumption of ore rocks under different loading waveforms *The Chinese Journal of Nonferrous Metals* **2**(4) 10-14 (in Chinese)
- [5] You Q M, Hua A Z 2002 Energy analysis on failure process of rock specimens *Chinese Journal of Rock Mechanics and Engineering* **21**(6) 778-781 (in Chinese)
- [6] Xia C J, Xie H P, Ju Y, Zhou H W 2006 Experimental study of energy dissipation of porous rock under impact loading *Engineering Mechanics* **23**(9) 1-5 (in Chinese)
- [7] L. Kong, Q. Su, Y.C. Wang, R. Peng 2012 Mesoscopic mechanics and energy dissipation analysis of sand deformation under slow cyclic loading. *Chinese Journal of Underground Space and Engineering* **8**(2), 268-273 (in Chinese)
- [8] Guo C Y, Xie X F, Wu X H, Yao W J, Zhang C Y 2008 The relationship among rock crushing energy, the Protodyakonov coefficient and rock strength *Journal of Chongqing Jianzhu University* **30**(6) 28-31 (in Chinese)
- [9] Goktan R M, Yilmaz N G 2005 A new methodology for the analysis of the relationship between rock brittleness index and drag pick cutting efficiency *Journal-south African Institute of Mining and Metallurgy* **105**(10) 727-733
- [10] Copur H, Bilgin N, Tuncdemir H, Balci C 2003 A set of indices based on indentation tests for assessment of rock cutting performance and rock properties *Journal-south African Institute of Mining and Metallurgy* **103** (9) 589-599
- [11] Adebayo B 2008 Evaluation of cuttability of selected rocks in south-western Nigeria *AU Journal of Technology* **12** (2) 126-129
- [12] Dey K, Ghose A K 2011 Review of Cuttability Indices and A new rockmass classification approach for selection of surface miners *Rock mechanics and rock engineering* **44**(5) 601-611
- [13] Tumac D, Bilgin N, Feridunoglu C, Ergin H 2007 Estimation of rock cuttability from shore hardness and compressive strength properties *Rock Mech. Rock Eng* **40**(5) 477-490
- [14] Krolczyk G, Legutko S, Stoić A 2013 Influence of cutting parameters and conditions onto surface hardness of Duplex Stainless Steel after turning process *Tehnički vjesnik – Technical Gazette* **20**(6) 1077-1080
- [15] Guettaf A, Chabane F, Arif A, Benramache S 2013 Dynamic Modeling in a Switched Reluctance Motor SRM using Finite Elements *Journal of Power Technologies* **93**(3) 149-153
- [16] Wang S R, Hagan P, Cheng Y 2012 Fractal Characteristics of Sandstone Cutting Fracture Under Mechanical Shock Loading Conditions *Applied Mechanics and Materials* **226-228** 1789-1794
- [17] Roxborough F F 1987 *The role of some basic rock properties in assessing cuttability. Seminar on Tunnels-Wholly Engineered Structures AFCC/IEAust Canberra, April, pp.1-21*

## Acknowledgments

This work was financially supported by the National Natural Science Foundation of China (51074140; 51310105020) and the Natural Science Foundation of Hebei Province of China (E2014203012), all these are gratefully acknowledged.

Authors	
	<p><b>Shuren Wang, born in December, 1968, Luannan County, Hebei Province, P.R. China</b></p> <p><b>Current position, grades:</b> Professor of School of Civil Engineering and Mechanics, Yanshan University, China.  <b>University studies:</b> received his Ph.D degree of Engineering Mechanics from University of Science and Technology Beijing, China.  <b>Scientific interest:</b> His research interest fields include mining engineering, geotechnical engineering, rock mechanics and numerical simulation analysis, etc.  <b>Publications:</b> more than 65 papers published in various journals.  <b>Experience:</b> He has working experience of 22 years, has completed 30 scientific research projects.</p>
	<p><b>Junqing Su, born in August, 1987, Mengcun County, Hebei Province, P.R. China</b></p> <p><b>Current position, grades:</b> Now he is a master student at School of Civil Engineering and Mechanics, Yanshan University, China.  <b>University studies:</b> He received B.S. degree from School of Civil Engineering and Mechanics, Yanshan University, China.  <b>Scientific interest:</b> His interested research is mining engineering, rock mechanics, and numerical simulation analysis, etc.  <b>Publications:</b> 3 papers published in various journals.  <b>Experience:</b> He has completed 2 scientific research projects.</p>
	<p><b>Paul Hagan, born in February, 1958, Newcastle City, New South Wales, Australia</b></p> <p><b>Current position, grades:</b> Associate Professor of School of Mining Engineering, University of New South Wales, Australia  <b>University studies:</b> received his Ph.D degree of Mining Engineering from School of Mining Engineering, University of New South Wales, Australia  <b>Scientific interest:</b> His research interest fields include mining engineering, rock mechanics, etc.  <b>Publications:</b> more than 60 papers published in various journals and academic conferences.  <b>Experience:</b> He has over thirty years' experience including twelve years in the mining industry.</p>